Title
Monitoring tumor response during photodynamic therapy using near-infrared photon-migration spectroscopy.

Journal
Photochemistry and photobiology, 73(6)

ISSN
0031-8655

Authors
Pham, TH
Hornung, R
Berns, MW
et al.

Publication Date
2001-06-01

DOI
10.1562/0031-8655(2001)073<0669:mtrdpt>2.0.co;2

Photochemistry and Photobiology, 2001, 73(6): 669–677

Monitoring Tumor Response During Photodynamic Therapy Using Near-infrared Photon-migration Spectroscopy¶

Tuan H. Pham[1], René Hornung[1,2], Michael W. Berns[1], Yona Tadir[1] and Bruce J. Tromberg*[1]

[1]Laser Microbeam and Medical Program (LAMMP), Beckman Laser Institute and Medical Clinic, University of California, Irvine, CA and
[2]Department of Obstetrics and Gynecology, University Hospital Zurich, Switzerland

Received 3 August 2000; accepted 16 February 2001

ABSTRACT

Benzoporphyrin-derivative (BPD)–monoacid-ring A photodynamic therapy (PDT) was performed on subcutaneous tumor implants in a rat ovarian cancer model. In order to assess PDT efficacy the tumor and normal tissue optical properties were measured noninvasively prior to and during PDT using frequency-domain photon migration (FDPM). FDPM data were used to quantify tissue absorption and reduced scattering properties (given by the parameters μ_a and μ'_s, respectively) at four near-infrared (NIR) wavelengths (674, 811, 849 and 956 nm). Tissue physiologic properties, including the *in vivo* concentration of BPD, deoxy-hemoglobin (Hb), oxy-hemoglobin (HbO_2), total hemoglobin (TotHb), water (H_2O) and percent tissue hemoglobin oxygen saturation ($\%S_tO_2$), were calculated from optical property data. PDT efficacy was also determined from morphometric analysis of tumor necrosis in histologic specimens. All the measured tumor properties changed significantly during PDT. [Hb] increased by 9%, while [HbO_2], [TotHb] and $\%S_tO_2$ decreased by 18, 7 and 12%, respectively. Using histologic data we show that long-term PDT efficacy is highly correlated to mean BPD concentration in tumor and PDT-induced acute changes in [HbO_2], [TotHb] and $\%S_tO_2$ (correlation coefficients of 0.829, 0.817 and 0.953, respectively). Overall, our results indicate that NIR FDPM spectroscopy is able to quantify noninvasively and dynamically the PDT-induced physiological effects *in vivo* that are highly correlated with therapeutic efficacy.

INTRODUCTION

Photodynamic therapy (PDT)† is currently being evaluated as an adjuvant to surgery, radiotherapy and chemotherapy for the treatment of hyperplastic and neoplastic diseases. PDT is generally based on the enhanced retention of photosensitizer (PS) in certain tissues which can lead to a roughly 2–10-fold contrast between diseased *versus* normal structures(1–3). In the presence of oxygen the irradiation of PS-laden tissue with light of appropriate wavelength leads to tissue necrosis *via* oxidative damage to cells and vasculature (4,5). PDT efficacy therefore depends on the availability of PS, light and oxygen. The relationship between light dose and the supply of both PS and oxygen during PDT is tissue dependent, dynamic and poorly understood *in vivo.* Consequently, studies designed to evaluate quantitatively the depletion of oxygen and/or PS from the treated tumors may substantially improve our understanding of PDT mechanisms and lead to improved therapeutic strategies.

PDT parameters (*e.g.* light dose and PS concentration) used for treating a specific lesion may not be ideal for all tissues. In order to optimize PDT for a given tissue type it is important to characterize light and PS distribution *in vivo* as well as the physiologic response to PDT-mediated damage. Previously measured acute PDT effects include changes in tissue deoxy-hemoglobin (Hb), oxy-hemoglobin (HbO_2) and total hemoglobin (TotHb) concentration as well as water content [H_2O](6,7). In addition, alterations in percent tissue hemoglobin oxygen saturation ($\%S_tO_2$) ($\%S_tO_2 = [HbO_2]/([HbO_2] + [Hb]) \times 100\%$) during light delivery are critical for assessing the hemodynamics and tissue oxygen consumption during PDT (8–10).

Frequency-domain photon migration (FDPM) uses intensity-modulated near-infrared (NIR) light to quantify noninvasively the tissue optical properties, namely the light absorption (μ_a) and reduced scattering (μ'_s) parameters. μ_a and μ'_s are sensitive to biologically important light-absorbing molecules and light-scattering structures, respectively. Intrinsic NIR-absorbing molecules in tissues are generally assumed to be hemoglobin (Hb and HbO_2), water, fat, cytochromes and melanin (11,12). μ_a is also sensitive to the concentration of NIR-absorbing drugs such as PS (13,14). Thus, FDPM measurements of wavelength-dependent absorption

¶Posted on the website on 28 February 2001.

*To whom correspondence should be addressed at: Laser Microbeam and Medical Program (LAMMP), Beckman Laser Institute and Medical Clinic, University of California, 1002 Health Sciences Road East, Irvine, CA 92612, USA. Fax: 949-824-6969; e-mail: tromberg@bli.uci.edu

†*Abbreviations:* BPD, benzoporphyrin derivative; DC direct current; Hb, deoxy-hemoglobin; HbO_2, oxy-hemoglobin; FDPM, frequency-domain photon migration; mean-$[BPD]_{PDT}$, mean BPD concentration in tumor during PDT; NIR, near-infrared; PBS, phosphate-buffered saline; PDT, photodynamic therapy; PDW, photon-density waves; PS, photosensitizer; SD, standard deviation; $\%S_tO_2$, percent tissue hemoglobin oxygen saturation; TotHb, total hemoglobin.

can be used to quantify the *in vivo* molecular concentration. These values are clinically useful indicators of tissue oxygen utilization, hydration and drug pharmacokinetics. Light scatterers are tissue-structural elements that have a dimension comparable to the optical wavelength (*e.g.* ~600–1000 nm), such as connective fibers in the extracellular matrix (*e.g.* collagen, elastin) and cellular components (15–17). Measurements of wavelength-dependent scattering properties offer insight into the composition, density and organization of tissue structures. Consequently, changes in the wavelength-dependent scattering properties may accompany processes such as malignant transformation, necrosis and wound healing (18–20).

In this work we examine how tissue optical properties can be used to assess noninvasively the PDT-mediated damage. Specific goals of the study were two-fold: (1) to determine the feasibility of using FDPM for dynamically monitoring PDT-induced changes in tissue benzoporphyrin derivative (BPD), hemoglobin, H_2O, $\%S_tO_2$ and μ'_s; and (2) to correlate the FDPM-derived values with histologic data in order to identify measurable parameters that may be used to predict PDT efficacy.

MATERIAL AND METHODS

Tumor model. Fourteen pathogen-free female Fischer 344 rats (Harlan Sprague Dawley, Inc., Indiana) weighing 194 g (±17 SD) were used. The animals were housed in a pathogen-free animal facility and given commercial basal diet and water *ad libitum.* The study was approved by the Institutional Laboratory Animal Care and Use Committee, University of California, Irvine, CA.

The NuTu-19 cell line is a poorly differentiated Fischer 344 rat–derived epithelial ovarian cancer cell line (21). This syngeneic rat tumor model was chosen because these cells grow and metastasize in the same way as epithelial ovarian cancers in humans (22). Cells were cultured in Roswell Park Memorial Institute 1640 medium (GIBCO Life Technologies, Grand Island, NY) enriched with 10% fetal calf serum (Gemini Bioproducts, Calabassas, CA), 25 IE/mL penicillin and 25 mg/mL streptomycin and incubated under standardized conditions (37°C, 7% CO_2, 100% humidity). The NuTu-19 cells were harvested with 0.25% trypsin (GIBCO) from tissue-culture flasks and washed with phosphate-buffered saline (PBS) (GIBCO). Twenty million cells were injected subcutaneously on the back of each rat. All procedures were carried out under isoflurane (Forane, Ohmeda PPD Inc., Liberty Corner, NJ) oxygen gas anesthesia. During all the procedures the body temperature of the rats was kept constant with a heating pad. Tumor growth was monitored with a caliper on a weekly basis.

PDT. Vials of liposomally formulated BPD (QLT PhotoTherapeutics, Inc., Vancouver, BC, Canada) were stored in the dark at 4°C before equilibration to room temperature and reconstitution to 2 mg/mL in 5% glucose solution. Four weeks following tumor induction, when bulky tumors had developed, nine rats were injected with 2 mg/kg BPD in the tail vein. Eighty minutes after BPD administration PDT laser light was delivered on to the tumor. The back of the rats was shaved prior to laser-light delivery. Laser light was generated by an argon-pumped dye laser (Spectra-Physics 171 and Spectra-Physics Model 375, Mountain View, CA). The laser was tuned to 692 nm and verified with a clinical Hartridge reversion spectroscope (Ealing Electro-Optics, South Natick, MA). The power was measured with a power meter (Model 210; Coherent Corp., Palo Alto, CA) prior to and after illumination and kept constant at 25 mW. The laser beam was conducted through a laser fiber terminated by a microlens and launched to the site of irradiation. The tip of the laser fiber was mounted above the tumor, perpendicular to the animal, allowing constant irradiation of a round 5 mm spot on the tumor. Laser light (25 mW) was administered to the tumors of the nine rats, sensitized with BPD for 5 min, to deliver a total fluence of 38.2 J/cm^2.

Frequency-domain photon migration. The theory and instrumentation of the FDPM approach to quantify the tissue optical properties are described in detail elsewhere (23–25). Briefly, FDPM launches the sinusoidally intensity–modulated NIR light into highly scattering tissues. Sinusoidally intensity–modulated light propagates in tissues as highly damped diffuse photon-density waves (PDW) with well-defined wave characteristics, specifically phase velocity and decay rate (26). PDW characteristics depend highly on the optical properties of the media. Measurements of frequency-dependent phase shift and amplitude decay of diffusely reflected PDWs can be fitted to analytically derived model functions to calculate tissue μ_a and μ'_s. The wavelength-dependent absorption was used to determine the tissue concentration of Hb, HbO_2, BPD and H_2O. Measured [Hb] and [HbO_2] were used to determine the TotHb concentration ([TotHb] = [Hb] + [HbO_2]) and oxygen saturation ($\%S_tO_2$).

For this study a portable broad-bandwidth FDPM instrument was used to quantify the tissue optical properties at multiple NIR wavelengths. FDPM measurements were performed using a probe with a source–detector separation of 9.45 mm. Both the source and detecting fibers were gently placed on the tissues to collect the FDPM data set which consists of phase and amplitude data for the wavelengths at 674, 811, 849 and 956 nm. Fibers were placed on the tumor and positioned in such a way as to obstruct minimally the PDT light. Typically, the PDT irradiation area was between the FDPM source and detecting fibers. Figure 1 is a schematic depiction of the FDPM instrument and the setup used to perform NIR frequency-domain spectroscopy in conjunction with PDT.

In order to evaluate the impact of BPD on absorption repeated injections of 2 mg/kg were administered into the tail vein of two tumor-free rats to reach a total dose of 20 mg/kg. Two minutes following the injection of each bolus FDPM measurements were performed on the back muscles of the rats. Optical properties of tissues at the four wavelengths were extracted from the FDPM data. Spectral-dependent absorption, in turn, was used to determine the physiologic properties. FDPM-derived BPD *in vivo* concentrations of the two rats were correlated to the injected BPD doses and compared to the published values obtained from radioactive labeled studies of BPD biodistributions (27).

FDPM measurements of normal and tumor optical properties were collected from six of the nine rats in the PDT group and one of the three tumor-bearing rats in the control group. Measurements of tumor properties were performed by positioning the FDPM probe over the subcutaneous tumor, while measurements of normal tissue were obtained from the anatomic site that mirrored the tumor. FDPM measurements of normal and tumor tissues were performed: (1) prior to PDT to establish the baseline properties; (2) following BPD administration to determine the BPD concentrations in tumor; and (3) during PDT to quantify the PDT-induced changes in optical properties. Five sets of FDPM data were collected on the normal and tumor sites for the baseline measurements. During PDT the FDPM data were collected continuously over the tumor site.

Concentrations. μ_a and μ'_s of normal and tumor tissues at the four wavelengths were extracted from the FDPM data sets. Wavelength-dependent absorption properties were then used to determine the concentrations ([Hb], [HbO_2], [H_2O] and [BPD]) for normal and tumor tissues. Specifically, concentrations and tissue-absorption values are related through the molar extinction coefficients ϵ by the following relation:

$$\begin{bmatrix} \mu_{647} \\ \mu_{811} \\ \mu_{849} \\ \mu_{956} \end{bmatrix} = \begin{bmatrix} \epsilon_{Hb}^{674} & \epsilon_{HbO_2}^{674} & \epsilon_{H_2O}^{647} & \epsilon_{BPD}^{674} \\ \epsilon_{Hb}^{811} & \epsilon_{HbO_2}^{811} & \epsilon_{H_2O}^{811} & \epsilon_{BPD}^{811} \\ \epsilon_{Hb}^{849} & \epsilon_{HbO_2}^{849} & \epsilon_{H_2O}^{849} & \epsilon_{BPD}^{849} \\ \epsilon_{Hb}^{956} & \epsilon_{HbO_2}^{956} & \epsilon_{H_2O}^{956} & \epsilon_{BPD}^{956} \end{bmatrix} \cdot \begin{bmatrix} [Hb] \\ [HbO_2] \\ [H_2O] \\ [BPD] \end{bmatrix}. \quad (1)$$

The extinction coefficients for Hb, HbO_2 and H_2O were from published values (11), while ϵ for BPD was determined from the absorption spectrum of BPD dissolved in 50% methanol–PBS solvent. The absorption spectrum of BPD from 500 to 1000 nm was measured using a UV–Vis–NIR spectrophotometer (DU630; Beckman Instruments, Inc., Fullerton, CA). Least square analysis was used to solve Eq. 1, with the constraint that the concentrations must be greater than zero (28). This approach ensures that a physically plausible solution exists even when there is uncertainty in the absorption val-

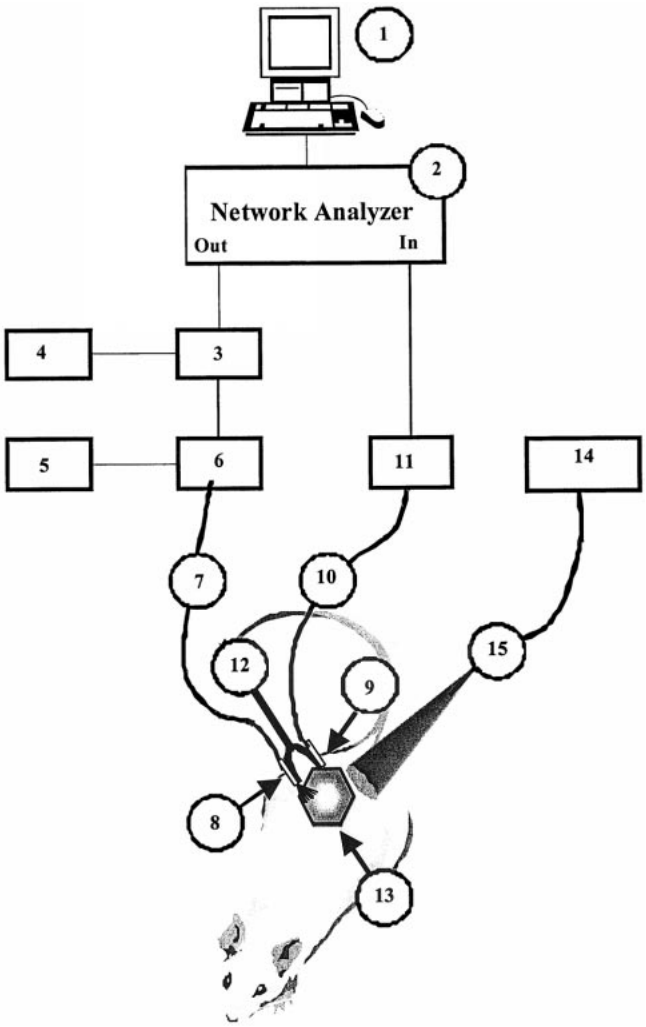

Figure 1. Schematic showing FDPM measurements performed in conjunction with PDT. The FDPM instrument consists of these principle components: (1) computer; (2) network analyzer; (3) bias-tee; (4) DC controller for diode lasers; (5) temperature controller for diode lasers; (6) four NIR diode lasers; (7) 674, 811, 849 and 956 nm optical fiber for light source; (8) tip of source fiber; (9) detecting tip; (10) optical fiber for signal detection; (11) avalanche photodiode; and (12) FDPM probe which consists of (7) source; and (10) detector optical fibers positioned 9.45 mm apart. The probe was placed gently on a (13) tumor that was subcutaneously implanted on the back of the rat. The tumor was irradiated with PDT light at 692 nm, which was generated from the (14) dye laser and coupled into the (15) PDT optical fiber.

ues from the different wavelengths. Moreover, least squares with positive constraint were empirically found to be robust in extracting dye concentrations of Intralipid-based phantoms (29,30).

Morphometry. Three days following PDT the rats were sacrificed with an intracardiac injection of Eutha-6 (Western Medical Supply, Arcadia, CA). Nine tumors exposed to PDT and three untreated tumors (controls) were collected (including the overlying skin). Each was fixed in 10% formalin for 24 h, dehydrated in graded ethylene alcohol, cleared in Histo-Clear (National Diagnostics, Manville, NJ), embedded in paraffin, sectioned perpendicularly to the skin in 6 μm slices, deparaffinized and stained with hematoxylin and eosin. On the serial sections through the entire area exposed to PDT central slides with the most extensive areas of necrosis were selected for analysis. Morphometry was performed on five central sections, each 60 μm apart. PDT damage was defined as the area of necrosis including severe perinecrotic inflammatory reaction The margins of

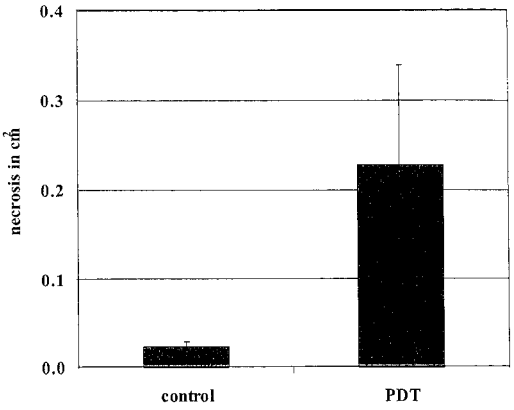

Figure 2. Results of morphometric analysis of the PDT effect on tumors shown for untreated control (n = 3) and PDT-treated (n = 9) rats. BPD was administered to the control and PDT-treated rats; however, only treated rats received PDT irradiation. Following systemic application of BPD (2 mg/kg) the tumors were irradiated at a fluence rate of 127 mW/cm^2 to give a total fluence of 38.2 J/cm^2. Area of necrosis (cm^2) is indicative of PDT efficacy. Data are presented as mean values ± SD (error bars).

PDT effect were marked with a permanent marker. The histology slides and a ruler were scanned (Umax Vista-SGE, Umax Data Systems Inc., Hsinchu, Taiwan; Photoshop, Adobe Systems Inc., Mountain View, CA) into a computer. The area of PDT-induced damage was measured using centimeter-calibrated IPlab software (Signal Analytic, Vienna, VA). The areas of five sections per tumor were measured and averaged, and 'PDT efficacy' is defined by the extent of PDT-mediated tissue necrosis.

Analysis of data. Mean damage area (±SD) was calculated from morphometry data of the PDT and control groups. μ_a, μ'_s, [Hb], [HbO_2], [TotHb], %S_tO_2, [H_2O] and [BPD] values from all the rats were combined and grouped into normal, tumor prior to PDT and tumor during PDT. Mean and SD of the optical and physiologic properties were calculated for each group. Morphometry data were correlated to mean tumor [BPD] as well as to PDT-induced changes in the tumor physiologic properties. Specifically, the correlation coefficient and confidence intervals were determined for: (1) efficacy *versus* mean tumor [BPD]; and (2) efficacy *versus* changes in TotHb and %S_tO_2, denoted by Δ[TotHb] and Δ%S_tO_2, respectively. All confidence intervals are specified for 95% limits. The unpaired *t*-test was used to determine the statistical significance for the difference between the mean areas of necrosis of untreated tumors *versus* the area of necrosis of PDT-treated tumors. The paired *t*-test was performed to calculate the statistical-significance difference for the following comparisons: (1) optical properties of normal *versus* optical properties of tumor prior to PDT; (2) optical properties of tumor prior to PDT *versus* optical properties of tumor during PDT; (3) physiologic properties of normal *versus* physiologic properties of tumor prior to PDT; and (4) physiologic properties of tumor prior to PDT *versus* physiologic properties of tumor during PDT. *P* values <0.05 were considered significant, while *P* values <0.005 were considered highly significant.

RESULTS

Photodynamic therapy

Four weeks following the injection of the NuTu-19 ovarian cancer cells the tumor nodules reached 14 mm (±3 mm SD) in diameter as measured *in vivo* with a caliper. The effect of PDT (38.2 J/cm^2) on tumors is shown in Fig. 2, which plots the area of necrosis (cm^2) for the control (n = 3) and PDT (n = 9) groups. The tumors treated with PDT showed significantly more necrosis than the untreated tumors ($P < 0.05$). The limited extent of necrosis in the untreated controls

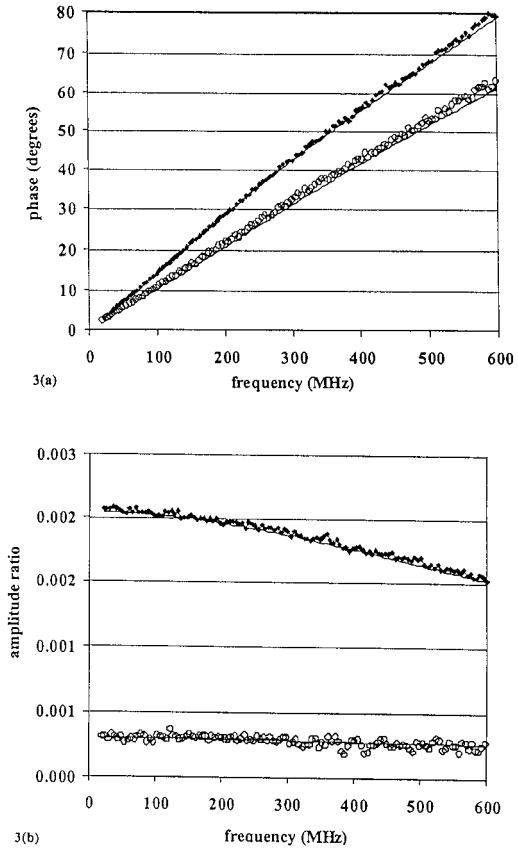

Figure 3. Example of FDPM phase (a) and amplitude (b) data at 674 nm collected from the tumor. Model functions are fit to the data to extract tissue absorption and reduced scattering coefficients. Data marked by diamonds (♦) were collected prior to BPD administration, while data marked by circles (○) were collected after 20 mg/kg of BPD was administered but prior to PDT. Lines are the results of the fit to the data.

is commonly observed in the rapidly growing solid tumors due to metabolic demands that outpace the vascular supplies.

Frequency-domain photon migration

An example of FDPM phase and amplitude data is shown in Fig. 3. Model functions were fit to PDW phase (Fig. 3a) and amplitude (Fig. 3b) to determine the tissue optical properties. Model functions (curves) fit well to the phase and amplitude data, with normalized χ^2 typically less than 1.8. FDPM data marked by diamonds were collected prior to BPD administration, while data marked by circles were collected following 4 mg of BPD. Representative μ_a and μ'_s of the four wavelengths are shown in subplots Fig. 4a,b, respectively, as a function of BPD-injected dose. Because the extinction coefficient of BPD at 674 nm is considerably higher than those at the other wavelengths, μ_a at 674 nm was the most sensitive to the administered BPD dose, while μ_a at the other wavelengths remained relatively constant (Fig. 4a). μ'_s for all the wavelengths was independent of the BPD dose, suggesting that the PS did not alter the tissue scattering.

Wavelength-dependent μ_a values were used to determine the physiologic properties including the BPD *in vivo* concentration. The FDPM-derived BPD *in vivo* concentration is

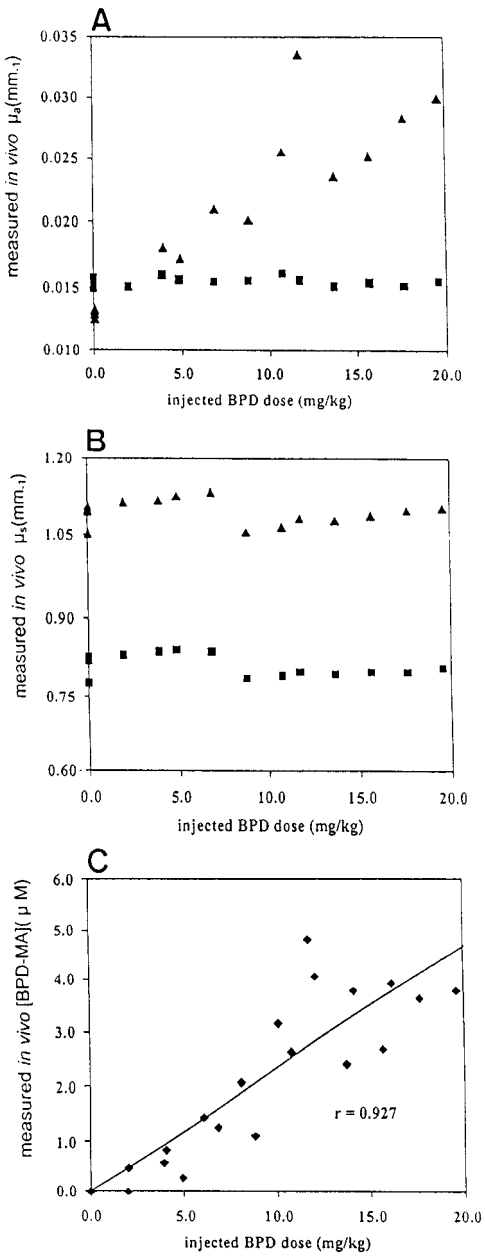

Figure 4. Tissue μ_a and μ'_s at 674 and 849 nm from one animal are shown as a function of administered BPD dose (mg/kg) in panels (a) and (b), respectively. FDPM measurements were collected 2–3 min following injection of BPD. In panel (a) μ_a at 674 nm (▲) increased markedly with BPD dose. Absorption at 849 nm (■) and other wavelengths remained relatively constant. μ'_s values at all wavelengths remained relatively constant as shown in panel (b) for 674 (▲) and 849 nm (■). Wavelength-dependent μ_a was used to calculate BPD concentration and physiologic properties. FDPM-derived *in vivo* BPD concentrations *versus* administered BPD dose are shown in panel (c) for data pooled from two animals. The correlation coefficient between measured [BPD] and administered BPD dose is 0.927, with a 95% confidence interval of (0.847,0.966) for n = 28 data points.

plotted *versus* the BPD-injected dose in panel (c) of Fig. 4; the subplot shows the data combined from two rats. Analysis of the correlation between the FDPM-derived [BPD] and the injected BPD dose yields a coefficient of 0.927, with a confidence interval of 0.847, 0.966. The slope of the line in Fig.

Table 1. Mean and standard deviation of optical properties (μ_a, μ_s') for normal tissue and malignant tumor prior to PDT (n = 7)

Wavelength (nm)	Normal tissue		Tumor prior to PDT	
	Mean	SD (±)	Mean	SD (±)
Absorption properties (μ_a) (mm^{-1})				
674	0.0144	0.0013	0.0163	0.0020
811	0.0360	0.0015	0.0374	0.0014
849	0.0145	0.0005	0.0153	0.0004
956	0.0300	0.0010	0.0304	0.0011
Scattering properties (μ_s') (mm^{-1})				
674	1.1391	0.0718	1.1125	0.0770
811	0.8906	0.0319	0.8606	0.0294
849	0.7325	0.0621	0.7140	0.0626
956	0.6404	0.0496	0.6161	0.0452

4c produces the calibration factor between the BPD-injected dose and the FDPM-derived [BPD] immediately following administration; the conversion factor for a 200 g rat is approximately 1.16 μM of BPD/1 mg of administered BPD dose.

The mean and SD of the optical properties are summarized in Table 1 for normal tissue and tumor prior to PDT. Mean absorption values of tumor are higher than those of normal tissues at all four wavelengths, with the largest percentage difference of 13% at 674 nm. Mean scattering values of normal tissues are higher than those of tumors, with the highest percentage difference of 4% at 956 nm. The mean scattering values decrease with longer wavelengths, which is an expected trend for most tissues.

Statistically significant differences in the optical properties between: (1) normal *versus* tumor prior to PDT; and (2) tumor prior to PDT *versus* tumor during PDT are summarized in Table 2. The μ_a value of tumor prior to PDT differed significantly from that of normal at all wavelengths ($P \leq 0.0293$) except at 956 nm ($P = 0.4625$). The μ_s' values of tumor differed significantly from those of normal at 674 and 811 nm ($P \leq 0.0447$) but not at 849 and 956 nm ($P \geq 0.2891$). Similarly, comparison of tumor μ_a values prior to PDT *versus* those during PDT showed statistically significant changes at all wavelengths ($P \leq 0.0298$) except at 956 nm ($P = 0.1824$). PDT did not induce statistically significant alterations in tumor μ_s' at any of the measured wavelengths ($P \geq 0.2691$).

Table 2. Paired *t*-test comparison of optical properties between normal tissue *versus* malignant tumor prior to PDT and malignant tumor prior to PDT *versus* malignant tumor during PDT

Wavelength (nm)	Normal *versus* tumor prior to PDT (n = 7)		Tumor prior to PDT *versus* tumor during PDT (n = 6)	
	Significance level*	*P* value	Significance level*	*P* value
Absorption coefficient (μ_a)				
674	s	0.0021	hs	0.0006
811	s	0.0293	s	0.0195
849	s	0.0017	s	0.0298
956	ns	0.4625	ns	0.1824
Scattering coefficient (μ_s')				
674	s	0.0447	ns	0.4877
811	s	0.0178	ns	0.8339
849	ns	0.4925	ns	0.6370
956	ns	0.2891	ns	0.2691

*hs = highly significant with $P < 0.005$; s = significant with $P < 0.05$ and ns = not significant with $P > 0.05$.

Table 3. Mean and standard deviation of physiologic properties for normal tissue, malignant tumor prior to PDT and malignant tumor during PDT

Physiologic properties	Normal tissue		Tumor (prior to PDT)		Tumor (during PDT)	
	Mean*	SD (±)	Mean*	SD (±)	Mean†	SD (±)
Hb (μM)	17.9	2.0	22.1	3.2	24.2	2.7
HbO_2 (μM)	34.1	1.7	34.6	1.5	28.4	2.9
TotHb (μM)	52.1	2.2	56.7	2.4	52.6	4.0
S_tO_2 (%)	65.6	3.1	61.2	4.3	54.0	3.8
H_2O (M)	24.2	1.1	24.0	1.5	23.4	1.4

*n = 7 (one from control and six from PDT group).
†n = 6 from PDT group.

The mean physiologic properties of normal tissues, tumor prior to PDT and tumor during PDT are summarized in Table 3, while Table 4 summarizes the *t*-test results for comparison of the physiologic properties. [Hb] and [TotHb] of tumor were significantly higher ($P \leq 0.00086$) than those of normal tissue, while the values for [HbO_2] were similar for tumor and for normal ($P = 0.42697$). Consequently, the mean %S_tO_2 values were significantly lower ($P = 0.00562$) in tumor (61.2 ± 4.3%) as compared with normal tissue (65.6 ± 3.1%). [H_2O] in tumor and normal tissues was comparable ($P = 0.56253$).

PDT-mediated effects on tumor can be observed by comparing the physiologic properties of untreated *versus* PDT-treated tumor as summarized in Tables 3 and 4. Mean [HbO_2] and [TotHb] in tumor during PDT decreased by a considerable amount from the untreated values ([HbO_2]: 34.6 ± 1.5 μM *versus* 28.4 ± 2.9 μM; [TotHb]: 56.7 ± 2.4 μM *versus* 52.6 ± 4.0 μM), while the concentration of Hb increased slightly (22.1 ± 3.2 μM *versus* 24.2 ± 2.7 μM). These changes resulted in the tumor %S_tO_2 values decreas-

Table 4. Paired *t*-test comparison of physiologic properties between normal tissue *versus* malignant tumor prior to PDT; and malignant tumor prior to PDT *versus* malignant tumor during PDT

Physiologic properties	Normal *versus* tumor prior to PDT (n = 7)		Tumor prior to PDT *versus* tumor during PDT (n = 6)	
	Significance level*	*P* value	Significance level*	*P* value
Hb (μM)	hs	0.00086	s	0.01338
HbO_2 (μM)	ns	0.42697	hs	0.00240
TotHb (μM)	hs	0.00003	s	0.02715
S_tO_2 (%)	s	0.00562	hs	0.00029
H_2O (M)	ns	0.56253	ns	0.38078

*hs = highly significant with $P < 0.005$, s = significant with $P < 0.05$ and ns = not significant with $P > 0.05$.

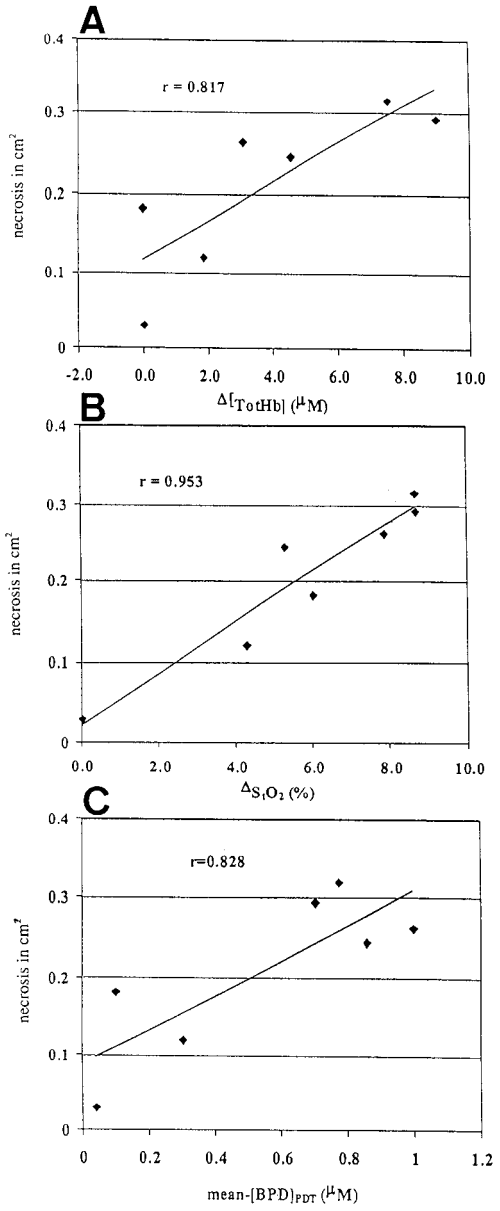

Figure 5. Area of necrosis (efficacy) is plotted as a function of PDT-induced changes in TotHb (Δ[TotHb]) in panel (a). Panel (b) plots efficacy *versus* changes in $\%S_tO_2$ ($\Delta\%S_tO_2$) and panel (c) plots efficacy *versus* mean BPD concentration in tumor during PDT (mean-$[BPD]_{PDT}$). Correlation coefficient (*R*) was calculated for each relationship and shown on the plots. Correlation coefficient is highest between efficacy and $\Delta\%S_tO_2$.

ing during PDT (61.2 ± 4.3% *versus* 54.0 ± 3.8%). PDT-induced changes in tumor [Hb], [HbO_2], [TotHb] and $\%S_tO_2$ were determined to be statistically significant ($P \leq 0.02715$). Mean [H_2O] remained unchanged during PDT.

In order to identify the physiologic parameters that may have prognostic value in predicting tumor response to PDT the FDPM data were correlated to histology-derived necrosis measurements. The factors that showed significant correlation to PDT efficacy are plotted in Fig. 5. Specifically, panel (a) of Fig. 5 plots the necrosis area *versus* the PDT-induced perturbations in Δ[TotHb], *i.e.* [TotHb] prior to PDT minus [TotHb] during PDT. Similarly, Fig. 5b,c shows the relationship between the necrosis area and the PDT-induced changes in tumor oxygen saturation, $\Delta\%S_tO_2$ (Fig. 5b) and mean [BPD] (Fig. 5c). The strongest correlation was observed between the necrosis area and $\Delta\%S_tO_2$, with $R = 0.953$ (0.708, 0.993). Correlation coefficients and confidence intervals for all three parameters are summarized in Table 5.

Table 5. Correlation coefficients for FDPM-derived parameters (Δ[TotHb], $\Delta\%S_tO_2$ and mean-BPD concentrations during PDT) that exhibited significant association with the efficacy of BPD-mediated PDT of malignant ovarian cell-line tumor (n = 7)

Correlation paramaters	Correlation coefficient (r)	95% confidence
Efficacy and Δ[TotHb] (μ*M*)	0.817	(0.166, 0.972)
Efficacy and $\Delta\%S_tO_2$ (%)	0.953	(0.708, 0.993)
Efficacy and mean-$[BPD]_{PDT}$	0.829	(0.201, 0.974)

DISCUSSION

Epithelial ovarian carcinoma is the leading cause of death from gynecological malignancies (31). The mainstay of treatment is surgical exploration and tumor debulking since survival is significantly improved when optimal surgical cytoreduction can be achieved prior to adjuvant chemotherapy (32,33). Unfortunately, two-thirds of the patients with advanced ovarian cancer cannot be optimally debulked (34) because of unresectable, bulky tumors and the diffuse intraperitoneal spread of solid cancer nodules (35). Hence, there is a strong need to develop new treatment and diagnostic modalities for the advanced stages of ovarian cancer. BPD-mediated PDT has recently been proposed as a treatment of the diffuse, solid intraperitoneal metastasis of ovarian cancer (36). However, the parameters of light and drug delivery to a very large surface such as the human peritoneum must be optimized for selectivity, efficacy and minimal surgery time.

PDT has been shown to induce acute physiologic responses, including vasoconstriction, vasodilation and edema (19,37,38). The characterization of PDT-induced physiologic responses may provide practical prognostic indicators of efficacy as well as insight into the PDT mechanisms. In this pilot study we performed PDT on ovarian-line tumors in a rat model. BPD was selected because it is a highly efficient PS (39) and exhibits a strong absorption peak at 692 nm (27,40) with a full-width half-maximum of ±10 nm.

In order to simplify data collection we performed FDPM measurements continuously during PDT irradiation. Despite this, there was no detectable contribution from either the PDT source or the 674 nm–excited BPD fluorescence to the FDPM signals. This is due to the fact that the FDPM instrument uses an alternate current–coupled avalanche photodiode and heterodyne detection to record radio-frequency modulated light while rejecting the time-independent signals (direct current [DC]). Nevertheless, the 692 nm illumination increases the detector-shot noise, resulting in higher phase and amplitude uncertainties during PDT irradiation.

It is also possible that FDPM-signal alterations may occur due to 674 nm–excited BPD fluorescence. If the fluorescence contribution to FDPM signals is significant, the data at modulation frequencies corresponding to the fluorescence life-

time would acquire an additional phase shift. Moreover, fluorescence contamination of FDPM data would lead to increasing amplitude and phase with higher BPD concentration. This is because the fluorescence-signal amplitude is proportional to [BPD], especially in the regime of low fluorophore concentration. For BPD, with a fluorescence lifetime of ~5 ns (41), the fluorescence effects on FDPM signals would be most apparent below ~70 MHz. Panels (a) and (b) of Fig. 3 show FDPM phase and amplitude data collected after the highest dose of 4 mg was administered (open circles). At high [BPD] the phase clearly increases monotonically without inflection at frequencies below 70 MHz. When the FDPM data were fit using frequencies above 100 MHz, μ_a and μ'_s were unchanged as compared with the values obtained by fitting the data to all frequencies. Furthermore, FDPM amplitude at frequencies below 70 MHz decreased monotonically with increasing BPD dose. These observations clearly suggest that the small BPD-fluorescence contribution to FDPM data did not affect the calculated optical property values.

The measured *in vivo* [BPD] was highly correlated to the administered BPD dose. Furthermore, the absolute values of FDPM-derived [BPD] were in excellent agreement with previous studies of BPD distribution in a mouse model (27). Specifically, at a dose of 2 mg/kg the typical FDPM-measured values of 1 μM for muscle correlate well with 0.5 μM (0.42 mg/g) from tritiated-label studies (27). Although not fully explored in this study, our data further suggest that FDPM measurements of PS concentration could be used to assess quantitatively the pharmacokinetics and biodistribution in tissues and hence the information about PS selectivity toward tumor.

A statistical comparison of [Hb], [TotHb], and $\%S_tO_2$ in normal *versus* malignant tumor revealed that [Hb] and [TotHb] were significantly elevated in tumor, while $\%S_tO_2$ was significantly lower. These findings are consistent with previous observations that malignant ovarian tumors are highly vascularized as compared to normal tissues (42–44) but tend to be in a hypoxic state because of the high metabolic demands (45,46). Statistical differences in μ_a of normal tissue *versus* tumor can be reasonably attributed to the physiologic difference observed between tissue types (Table 3). The μ'_s of normal sites were higher than those of tumor at all four wavelengths; however, differences were statistically significant only at 674 and 811 nm. Presumably, lower μ'_s values in tumor are due to variations in structural composition. For example, invasive tumors may have high cell density but low collagen content, resulting in an overall reduction in μ'_s since collagen is a prominent tissue scatterer (16).

Values for [HbO_2], [TotHb], and $\%S_tO_2$ decreased significantly from tumor baseline during PDT (Table 3). [Hb] increased during PDT while [H_2O] remained unchanged. The PDT-induced tissue response was statistically significant for all physiologic parameters with the exception of water (Table 4), and can be explained in terms of known PDT mechanisms.

Primary PDT effects involve the formation of reactive-oxygen intermediates, such as singlet molecular oxygen, which cause oxidative damage to the cells and vasculature. This rapidly leads to vasoconstriction and cell death *via* both necrotic and apoptotic pathways (47–49). BPD-mediated PDT, in particular, induces severe vasoconstriction, which has been directly observed using light microscopy (50,51) and optical coherence tomography (52). Evidence for the formation of reactive-oxygen intermediates has been shown to be coupled with the depletion of ground-state molecular oxygen (5). PDT-induced vasoconstriction decreases blood flow to the tumor, lowering the [TotHb]. Ischemia enhances the desaturation of [HbO_2] due to increased oxygen extraction from blood in low flow-rate vessels. The formation of singlet oxygen can also contribute to [HbO_2] desaturation since the photochemically driven depletion of dissolved oxygen that occurs during Type-II photooxidation creates an oxygen gradient that is resupplied by HbO_2. All of these processes result in a marked decrease in $\%S_tO_2$ and subsequent elevation of [Hb]. These acute PDT physiologic changes coincide with the significant differences between μ_a before and during PDT of tumor. μ'_s remains unaffected during PDT (Tables 1 and 2) due to the insensitivity of structural components to these short-term physiologic changes.

Although these acute PDT effects are dramatic and can be easily monitored, they do not necessarily predict the long-term outcome. However, since the alterations in FDPM-measured physiology are compatible with the known PDT mechanisms of toxicity, it is not unreasonable to expect these measured variables to be related to long-term efficacy. This is supported by the data in Fig. 5 which show excellent correlation between the histologically measured necrosis area and the FDPM measurements of: (1) Δ[TotHb]; (2) $\Delta\%S_tO_2$; and (3) mean BPD concentration in tumor during PDT (mean-$[BPD]_{PDT}$). We believe this is an important finding since it clearly demonstrates how FDPM could be used during treatment to report on a number of practical prognostic indicators. For example, the measurements of Δ[TotHb] or $\Delta[\%S_tO_2]$, and mean-$[BPD]_{PDT}$ might be used to provide rapid feedback for optimization of the PS dose, drug–light interval and light-administration protocol (*e.g.* fractionated *versus* continuous irradiation, dose *versus* dose–rate effects). When combined with other optical methods, such as PS-fluorescence bleach rate, a more complete picture of the complex relationship between drug and light dose should emerge which can be used to improve the therapeutic outcome for a given tissue type.

Acknowledgements—Support for this work was provided by the National Institutes of Health (NIH) to the Laser Microbeam and Medical Program (LAMMP; grant RR-01192), the Chao Comprehensive Cancer Center (CA-62203) and NIH grants GM-50958, CA-32248 and HD-34091. In addition, Beckman Laser Institute programmatic support from the Department of Energy (DOE DE-FG03-91ER61227), the Office of Naval Research (ONR N00014-91-C-0134) and the Beckman foundation is acknowledged. T.H.P. is grateful for support from the Whitaker Foundation Biomedical Engineering Graduate Fellowship. R.H. wishes to acknowledge the Swiss National Research Foundation, the Huggenberger-Bischoff Stiftung and the Theodor und Ida Herzog-Egli Stiftung.

REFERENCES

1. Gomer, C. J. and T. J. Dougherty (1979) Determination of [^{3}H] and [^{14}C]hematoporphyrin derivative distribution in malignant and normal tissue. *Cancer Res.* **39**, 146–151.
2. Chatlani, P. T., P. J. Nuutinen, N. Toda, H. Barr, A. J. MacRobert, J. Bedwell and S. G. Bown (1992) Selective necrosis in hamster pancreatic tumours using photodynamic therapy with phthalocyanine photosensitization. *Br. J. Surg.* **79**, 786–790.

3. Barr, H., C. J. Tralau, P. B. Boulos, A. J. MacRobert, N. Krasner, D. Phillips and S. G. Bown (1990) Selective necrosis in dimethylhydrazine-induced rat colon tumors using phthalocyanine photodynamic therapy. *Gastroenterology* **98**, 1532–1537.
4. Weishaupt, K. R., C. J. Gomer and T. J. Dougherty (1976) Identification of singlet oxygen as the cytotoxic agent in photo-inactivation of a murine tumor. *Cancer Res.* **36**, 2326–2329.
5. Kimel, S., B. J. Tromberg, W. G. Roberts and M. W. Berns (1989) Singlet oxygen generation of porphyrins, chlorins, and phthalocyanines. *Photochem. Photobiol.* **50**, 175–183.
6. Wieman, T. J., T. S. Mang, V. H. Fingar, T. G. Hill, M. W. R. Reed, T. S. Corey, V. Q. Nguyen and E. R. Render (1988) Effect of photodynamic therapy on blood flow in normal and tumor vessels. *Surgery* **104**, 512–517.
7. Fingar, V. H., T. J. Wieman, S. A. Wiehle and P. B. Cerrito (1992) The role of microvascular damage in photodynamic therapy: the effect of treatment on vessel constriction, permeability and leukocyte adhesion. *Cancer Res.* **52**, 4914–4921.
8. Henderson, B. W. and V. H. Fingar (1987) Relationship of tumor hypoxia and response to photodynamic treatment in an experimental mouse tumor. *Cancer Res.* **47**, 3110–3114.
9. Foster, T. H., R. S. Murant, R. G. Bryant, R. S. Knox, S. L. Gibson and R. Hilf (1991) Oxygen consumption and diffusion effects in photodynamic therapy. *Radiat. Res.* **126**, 296–303.
10. Foster, T. H. and L. Gao (1992) Dosimetry in photodynamic therapy: oxygen and the critical importance of capillary density. *Radiat. Res.* **130**, 379–383.
11. Cope, M. (1991) The application of near infrared spectroscopy to non-invasive monitoring of cerebral oxygenation in the newborn infant. Dissertation thesis, University College London, London, UK.
12. Duck, F. A. (1990) *Physical Properties of Tissue.* Academic Press, London.
13. Patterson, M. S., E. Schwartz and B. C. Wilson (1989) Quantitative reflectance spectrophotometry for the noninvasive measurement of photosensitizer concentration in tissue during photodynamic therapy. *Proc. Soc. Photo-opt. Instrum. Eng.* **1065**, 115–122.
14. Pottier, R. (1990) *In vitro* and *in vivo* fluorescence monitoring of photosensitizers. *J. Photochem. Photobiol. B: Biol.* **6**, 103–109.
15. Saidi, I. S., S. L. Jacques and F. K. Tittel (1995) Mie and Rayleigh modeling of visible-light scattering in neonatal skin. *Appl. Opt.* **34**, 7410–7418.
16. Dunn, A., C. Smithpeter, A. J. Welch and R. Richards-Kortum (1996) Light scattering from cells. *Biomedical Optical Spectroscopy and Diagnostics*, pp. 50–52. Proceedings of the Optical Society of America.
17. Mourant, J. R., J. P. Freyer, A. H. Hielscher, A. A. Eick, D. Shen and T. M. Johnson (1998) Mechanisms of light scattering from biological cells relevant to noninvasive optical-tissue diagnostics. *Appl. Opt.* **37**, 3586–3593.
18. Liu, D. L., S. Andersson-Engels, C. Sturesson, K. Svanberg, C. H. Håkansson and S. Svanberg (1996) Tumour vessel damage resulting from laser-induced hyperthermia alone and in combination with photodynamic therapy. *Cancer Lett.* **111**, 1–9.
19. Fehr, M. K., B. J. Tromberg, L. O. Svaasand, P. Ngo, M. W. Berns and Y. Tadir (1996) Structural and functional effects of endometrial photodynamic therapy in a rat model. *Am. J. Obstet. Gynecol.* **175**, 115–121.
20. Hornung, R., T. H. Pham, K. A. Keefe, M. W. Berns, Y. Tadir and B. J. Tromberg (1999) Quantitative near-infrared spectroscopy of cervical dysplasia in vivo. *Hum. Reprod.* **14**, 2908–2916.
21. Testa, J. R., L. A. Getts, H. Salazar, Z. Liu, L. M. Handel, A. K. Godwin and T. C. Hamilton (1994) Spontaneous transformation of rat ovarian surface epithelial cells results in well to poorly differentiated tumors with a parallel range of cytogenetic complexity. *Cancer Res.* **54**, 2778–2784.
22. Rose, G. S., L. M. Tocco, G. A. Grander, P. J. DiSaia, T. C. Hamilton, A. D. Santin and S. Hjerten (1996) Development and characterization of a clinically useful animal model of epithelial ovarian cancer in the Fischer 344 rat. *Am. J. Obstet. Gynecol.* **175**, 593–599.
23. Madsen, S. J., E. R. Anderson, R. C. Haskell and B. J. Tromberg (1994) Portable, high-bandwidth frequency-domain photon migration instrument for tissue spectroscopy. *Opt. Lett.* **19**, 1934–1936.
24. Fishkin, J. B., O. Coquoz, E. R. Anderson, M. Brenner and B. J. Tromberg (1997) Frequency-domain photon migration measurements of normal and malignant tissue optical properties in a human subject. *Appl. Opt.* **36**, 10–20.
25. Pham, T. H., O. Coquoz, J. B. Fishkin, E. Anderson and B. J. Tromberg (2000) A broad bandwidth frequency domain instrument for quantitative tissue optical spectroscopy. *Rev. Sci. Instrum.* **71**, 2500–2513.
26. Tromberg, B. J., L. O. Svaasand, T.-T. Tsay and R. C. Haskell (1993) Properties of photon density waves in multiple-scattering media. *Appl. Opt.* **32**, 607–616.
27. Richter, A. M., S. Cerruti-Sola, E. D. Sternberg, D. Dolphin and J. G. Levy (1990) Biodistribution of tritiated benzoporphyrin derivative (^{3}H-BPD–MA), a new potent photosensitizer, in normal and tumor-bearing mice. *J. Photochem. Photobiol. B: Biol.* **5**, 231–244.
28. Lawson, C. L. and R. J. Hanson (1974) *Solving Least Squares Problems.* Prentice-Hall, New York.
29. Pham, T. H., F. Bevilacqua, T. Spott, J. S. Dam, B. J. Tromberg and S. Andersson-Engels (2000) Quantifying the absorption and reduced scattering coefficients of tissue-like turbid media over a broad spectral range using a non-contact Fourier interferometric, hyperspectral imaging system. *Appl. Opt.* **39**, 6487–6497.
30. Pham, T. H., C. Eker, Tromberg B. J. and S. Andersson-Engels (2001) Quantifying the optical properties and chromophore concentrations of turbid media by chemometric analysis of hyperspectral, diffuse reflectance data collected using a Fourier interferometric imaging system. *Appl. Spectrosc.* (submitted)
31. Parker, S. L., T. Tong, S. Bolden and P. A. Wingo (1996) Cancer statistics, 1996. *CA—Cancer J. Clin.* **46**, 5–27.
32. Curtin, J. P., R. Malik, E. S. Venkatraman and W. J. Hoskins (1997) Stage IV ovarian cancer: impact of surgical debulking. *Gynecol. Oncol.* **64**, 9–12.
33. Munkarah, A. R., A. V. Hallum, M. Morris, T. W. Burke, C. Levenback, E. N. Atkinson, J. T. Wharton and D. M. Gershenson (1997) Prognostic significance of residual disease in patients with stage IV epithelial ovarian cancer. *Gynecol. Oncol.* **64**, 13–17.
34. Schwartz, P. E. (1997) Cytoreductive surgery for the management of stage IV ovarian cancer [editorial; comment]. *Gynecol. Oncol.* **64**, 1–3.
35. DiSaia, P. J. and W. Creasman (19997) Epithelial ovarian cancer. *Clinical Gynecologic Oncology* (Edited by P. J. DiSaia and W. Creasman), pp. 282–350. Mosby-Year Book, Inc., St. Louis.
36. Molpus, K., D. Kato, M. R. Hamblin, L. Lilge, M. Bamberg and T. Hasan (1996) Intraperitoneal photodynamic therapy of human epithelial ovarian carcinomatosis in a xenograft murine model. *Cancer Res.* **56**, 1075–1082.
37. Reed, M. W. R., F. N. Miller, T. J. Wieman, M. T. Tseng and C. G. Pietsch (1988) The effect of photodynamic therapy on the microcirculation. *J. Surg. Res.* **45**, 452–459.
38. Sigdestad, C. P., V. H. Fingar, T. J. Wieman and R. D. Lindberg (1996) Chemical modification of normal tissue damage induced by photodynamic therapy. *Br. J. Cancer* **27(Suppl.)**, s–s92.
39. Richter, A. M., B. Kelly, J. Chow, D. J. Liu, G. H. N. Towers, D. Dolphin and J. G. Levy (1987) Preliminary studies on a more effective phototoxic agent than hematoporphyrin. *J. Natl. Cancer Inst.* **79**, 1327–1332.
40. Allison, B. A., E. Waterfield, A. M. Richter and J. G. Levy (1991) The effects of plasma lipoproteins on *in vitro* tumor cell killing and *in vivo* tumor photosensitization with benzoporphyrin derivative. *Photochem. Photobiol.* **54**, 709–715.
41. Aveline, B., T. Hasan and R. W. Redmond (1994) Photophysical and photosensitizing properties of benzoporphyrin derivative monoacid ring A (BPD–MA). *Photochem. Photobiol.* **59**, 328–335.
42. Hollingsworth, H. C., E. C. Kohn, S. M. Steinberg, M. L. Rothenberg and M. J. Merino (1995) Tumor angiogenesis in advanced stage ovarian carcinoma. *Am. J. Pathol.* **147**, 33–41.

43. Abulafia, O., W. E. Triest and D. M. Sherer (1997) Angiogenesis in primary and metastatic epithelial ovarian carcinoma. *Am. J. Obstet. Gynecol.* **177**, 541–547.
44. Emoto, M., T. Udo, H. Obama, F. Eguchi, T. Hachisuga and T. Kawarabayashi (1998) The blood flow characteristics in borderline ovarian tumors based on both color Doppler ultrasound and histopathological analyses. *Gynecol. Oncol.* **70**, 351–357.
45. Milross, C. G., S. L. Tucker, K. A. Mason, N. R. Hunter, L. J. Peters and L. Milasm (1997) The effect of tumor size on necrosis and polarographically measured pO2. *Acta Oncol.* **36**, 183–189.
46. Rofstad, E. K., P. DeMuth and R. M. Sutherland (1988) 31P NMR spectroscopy measurements of human ovarian carcinoma xenografts: relationship to tumour volume, growth rate, necrotic fraction and differentiation status. *Radiother. Oncol.* **12**, 315–326.
47. Dougherty, T. J., C. J. Gomer, B. W. Henderson, G. Jori, D. Kessel, M. Korbelik, J. Moan and Q. Peng (1998) Photodynamic therapy. *J. Natl. Cancer Inst.* **90**, 889–905.
48. Henderson, B. W. and T. J. Dougherty (1992) *Photodynamic Therapy—Basic Principle and Clinical Applications.* Marcel Dekker, New York.
49. Nelson, J. S., L.-H. Liaw, A. Orenstein, W. G. Roberts and M. W. Berns (1988) Mechanism of tumor destruction following photodynamic therapy with hematoporphyrin derivative, chlorin, and phthalocyanine. *J. Natl. Cancer Inst.* **80**, 1599–1605.
50. Hornung, R., M. Hammer-Wilson, S. Kimel, L.-H. Liaw, Y. Tadir and M. W. Berns (1999) Systemic application of photosensitizers in the chick chorioallantoic membrane (CAM) model: photodynamic response of CAM vessels and 5-aminolevulinic acid uptake kinetics by transplantable tumors. *J. Photochem. Photobiol. B: Biol.* **49**, 41–49.
51. König, K., S. Kimel and M. W. Berns (1996) Photodynamic effects on human and chicken erythrocytes studied with microirradiation and confocal laser scanning microscopy. *Lasers Surg. Med.* **19**, 284–298.
52. Chen, Z., T. E. Milner, X. Wang, S. Srinivas and J. S. Nelson (1998) Optical Doppler tomography: imaging *in vivo* blood flow dynamics following pharmacological intervention and photodynamic therapy. *Photochem. Photobiol.* **67**, 56–60.